Comparative study of the pressure dependence of optical-phonon transverse-effective charges and linewidths in wurtzite InN

J. S. Reparaz,[1,*] K. Pereira da Silva,[1,2] A. H. Romero,[3,4] J. Serrano,[5] M. R. Wagner,[6] G. Callsen,[6] S. J. Choi,[7] J. S. Speck,[7] and A. R. Goñi[1,8,†]

[1]*Institut de Ciència de Materials de Barcelona-CSIC, Esfera UAB, 08193 Bellaterra, Spain*
[2]*Faculdade de Física, Universidade Federal do Pará, CEP 66075-110, Belém, Pará, Brazil*
[3]*Physics Department, West Virginia University, Morgantown, West Virginia 26506, USA*
[4]*Facultad de Ingeniería, Benemérita Universidad Autónoma de Puebla, 72570 Puebla, Puebla, Mexico*
[5]*Yachay Tech University, School of Physical Sciences and Nanotechnology, Urcuqu 100119, Ecuador*
[6]*Institut für Festkörperphysik, Technische Universität Berlin, Hardenbergstrasse 36, 10623 Berlin, Germany*
[7]*Materials Department, University of California, Santa Barbara, California 93106-5050, USA*
[8]*ICREA, Passeig Lluís Companys 23, 08010 Barcelona, Spain*

(Received 20 June 2017; revised manuscript received 9 July 2018; published 16 October 2018)

We investigate the hydrostatic pressure dependence of the zone center optical phonons of *c*-plane and *a*-plane wurtzite InN epilayers grown on GaN substrates. The longitudinal to transverse mode splitting for the A_1 and E_1 modes was found to increase with increasing pressure, whereas the associated transverse effective charge decreases for both modes as $e_T^*(A_1) = 2.93\text{–}9.9 \times 10^{-3} P$ and $e_T^*(E_1) = 2.80\text{–}10.6 \times 10^{-3} P$ (in units of elementary charge and P in GPa). These observations are well in line with results for other II–VI, III–V, and group-IV semiconductor compounds as far as the relation between the magnitude and sign of the pressure derivative of e_T^* and the bond ionicity is concerned. As the latter increases so does $|\partial e_T^*/\partial P|$ with a sign change from positive to negative for bond ionicities around $f_i = 0.46$ for compounds with anions belonging to the first row of the Periodic Table. A comparison of the results for InN and other nine tetrahedrally bonded compounds indicate that the pressure behavior of the transverse effective charge is mainly determined by the strength of the Pauli repulsion between cation valence electrons and those of the anion core. We also perform *ab initio* calculations in order to address the origin of the observed increase in linewidth of the E_2^{high} mode which is found to arise from a pressure-induced increase in the rate of two-phonon decay processes. This broadening is associated with tuning into resonance of a steep edge in the two-phonon density of states around 460 cm^{-1} with the frequency of the E_2^{high} mode.

DOI: 10.1103/PhysRevB.98.165204

I. INTRODUCTION

Group-III nitrides are particularly suitable for a variety of optoelectronic applications mainly due to the large versatility as optical emitters. Their fundamental band gap ranges from 0.7 eV for InN to 6.2 eV for AlN, spanning through this spectral window by alloying with Ga. From a lattice-vibration perspective these materials also show interesting properties, e.g., the lattice thermal conductivity of unintentionally doped substrates exhibits a 16-fold reduction: BN, AlN, GaN, InN $\rightarrow \kappa = 740, 285, 130, 45\ \text{Wm}^{-1}\,\text{K}^{-1}$, respectively [1]. Such a variation of their heat transport properties originates partially from their large atomic mass ratio between the cations ($m_{In}/m_B \approx 10.6$) or, in other words, from their very distinct phonon dispersion relation. The phonon spectrum of InN has been studied already some years ago by means of Raman scattering [2,3] and, more recently, using inelastic x-ray scattering [4]. At ambient conditions the thermodynamically stable phase of InN is found to be the wurtzite structure belonging to the space group C_{6v}^4 with four atoms per unit cell, which leads to six Raman active modes: E_2^{high} and E_2^{low} which originate from vibrations of the N and In sublattices, respectively; A_1(TO) and A_1(LO) with the atomic displacements parallel to the *c* axis; E_1(TO) and E_1(LO) with the atomic displacements perpendicular to the *c* axis, where TO and LO stands for transverse and longitudinal optical, respectively. Whereas the E_2 modes have a nonpolar character and are generally used to determine the strain, the E_1 and A_1 modes are intrinsically polar and, thus, their spectral position and linewidth might be affected by coupling to the background carrier concentration.

In polar lattices the fundamental quantity that determines the splitting of the polar modes, $\Delta\omega = \omega_{\text{LO}} - \omega_{\text{TO}}$, is the dynamical effective charge of the bonds e_T^*. This last quantity must not be confused with the static bond polarity (α_P) which results from the electronegativity of the ions constituting the bond. A direct experimental determination of e_T^* is by no means straightforward since it involves measuring the temporal average of a time dependent quantity which is reflected in the propagation of a phonon. However, it is possible to define its magnitude from the longitudinal to transverse mode splitting as follows:

$$e_T^* = \sqrt{\epsilon_0(\epsilon_\infty) V \mu \left[\omega_{\text{LO}}^2 - \omega_{\text{TO}}^2\right]}, \tag{1}$$

*Corresponding author: jsreparaz@icmab.es
†Corresponding author: goni@icmab.es

where ϵ_0 is the vacuum permittivity, ϵ_∞ is the high-frequency (or pure electronic) dielectric constant of the material, V is the volume per anion-cation pair, μ is the reduced mass of the pair, and ω_i is the mode dependent phonon frequency. The previous equation shows that the pressure dependence of e_T^* is given by three independent components: the splitting $\Delta\omega(P)$ of the optical modes, the screening term given by the dielectric constant $\epsilon_\infty(P)$, and the volume of the unit cell $V(P)$. Whereas $V(P)$ can be readily obtained from x-ray diffraction under hydrostatic pressure, the direct determination of $\epsilon_\infty(P)$ is usually achieved through optical interference experiments [5,6]. Finally, $\Delta\omega(P)$ is easily extracted from pressure dependent Raman-scattering measurements. Interestingly, the transverse effective charge of the optical modes for the series of compounds SiC [7], AlN [8], GaN [8], and ZnO [9] exhibited a clear trend of the pressure coefficient as a function of the bond polarity. The more ionic the material, the larger the transverse effective charge, whereas the pressure derivative of e_T^* turned from positive to more negative.

As far as the wurtzite phase on InN is concerned, the hydrostatic pressure dependence of the Raman modes was studied a decade ago in thin films with the crystal quality available at that time [2,10], leading to a somewhat inaccurate determination of their pressure coefficients. In particular, a clear observation of the LO modes that would allow a clear assignment to the A_1 or E_1 symmetry was not possible, hence, totally hampering the study of the transverse effective charges associated to the different modes. Improvements in nitride growth techniques yielded samples with better structural properties, allowing an accurate determination by Raman scattering of the frequencies of vibrational modes and their pressure dependence. For instance, in a recent work [11] a good agreement was found between measured and calculated pressure coefficients of zone-center optical modes. Finally, the same group published a more comprehensive experimental and theoretical lattice-dynamical study of InN in both the wurtzite and rocksalt structure performed by applying very high pressure up to 20 GPa [12]. In this work, the Raman measurements were carried out on samples with fairly high electron concentrations ranging from 1×10^{18} to 2×10^{19} cm^{-3}, which allowed the study of the pressure behavior of LO phonons with large wave vectors through the coupling to the free carriers, analyzed by considering the double-resonance mechanism proposed by Davydov *et al.* [13]. Nevertheless, neither the effects of pressure on optical-phonon effective charges or linewidths were addressed.

Here, we focus on the hydrostatic pressure dependence of the optical modes in wurtzite InN epilayers in the pressure range up to 8 GPa. Specifically, we were able to unravel the sign and magnitude of the pressure coefficient of the transverse effective charge of the A_1 or E_1 modes, having in mind the observed systematic in terms of the material ionicity mentioned above and by comparing with results obtained for nine other tetrahedrally bonded semiconductor compounds. We also disentangled the different contributions to the pressure derivative of e_T^* and show that for such a low band-gap material like InN the (positive) contribution from the splitting of the polar optical modes ($\Delta\omega$) is overcompensated by the strong reduction of the electronic dielectric constant (ϵ_∞) with increasing pressure [5]. Furthermore, with the help of *ab initio* calculations we studied the pressure dependence of the Raman linewidths. For instance, we observed that the E_2^{high} mode exhibits a characteristic Fano-like broadening due to large phonon anharmonicities, which can be understood in terms of the pressure tuning of a Fermi resonance, as reported for other semiconductors [14–16].

II. EXPERIMENTS AND SIMULATIONS

The samples were grown by plasma-assisted molecular beam epitaxy (PA-MBE) on a 100-nm-thick C-doped (semi-insulating) GaN buffer layer on a semi-insulating c-plane GaN:Fe template (Lumilog). The InN growth rate was 300 nm/h at a substrate temperature of 440–450 C (measured by pyrometer) under In-rich growth conditions. A carrier density of 5.2×10^{17} cm^{-3} was obtained. Raman spectra were collected with a LabRam HR800 system in backscattering geometry at room temperature using the 514.5-nm line of an Ar^+ laser, which was focused onto the sample using a long-distance 20× Olympus objective. Raman peak positions were determined with a spectral accuracy less than 0.1 cm^{-1}. For absolute wavelength calibration we have considered the Si LO mode at 520.7 cm^{-1}. Measurements under pressure were carried out using the diamond-anvil cell (DAC) technique. A 4:1 mixture of methanol and ethanol was employed as the pressure-transmitting medium. Pressure was monitored *in situ* by the shift of the ruby R_1 line [17]. Two InN epilayers grown in the c-plane and a-plane directions were thinned from the substrate side to about 30 μm by mechanical polishing and loaded into the DAC. In these configurations the c and a axes of the InN crystal is parallel to the direction of incidence of the laser light, thus resulting in different polarization geometries leading to different active Raman modes for each of them.

Ab initio lattice-dynamical calculations were performed within the framework of density functional theory (DFT) [18,19] and density functional perturbation theory (DFPT) [20], as implemented in the ABINIT code [18,21–23]. For the calculation of the dynamical properties (phonons) at ambient conditions and as a function of pressure we have used a regular q-point mesh of $6 \times 6 \times 3$ [19]. To describe the vibrational properties at the quasiharmonic level, the generalized gradient approximation (GGA) was used to set the exchange correlation functional with the Perdew-Burke-Ernzerhof (PBE) formalism [24]. The use of the linear-response method avoids the need of supercells and allows the calculation of the dynamical matrix at arbitrary q vectors. Further calculations of phonon linewidths, accounting for anharmonic two-phonon decay processes, were performed within the same exchange correlation functional. Though some authors have used the local-density approximation (LDA) to describe the vibrational properties, we have used GGA as it gives better results for the two phonon process and we want to be consistent throughout the paper. However, we note that the agreement between the theoretical and experimental values of phonon frequencies as well as the pressure coefficients is poorer for GGA as compared to LDA. Wave functions were described by using linear combinations of plane waves with norm conserving pseudopotentials [25]. We have discretized the reciprocal space with a regular k-point mesh of $8 \times 8 \times 4$, while we have chosen a cutoff energy for the expansion of plane waves of

50 Ha (1360 eV). With this optimization, we assure that the system was fully relaxed with forces between atoms no larger than 10^{-7} Ha/Bohr and that the stress of the crystal cell is as small as 10^{-5} GPa. We have used the Anaddb postprocessing utility provided within the ABINIT code to calculate the exact interatomic force constants (IFCs) for the defined points in the q mesh as well as to interpolate the IFCs for other points. From these constants, the atomic-projected one- and two-phonon densities of states (2PDOS) are calculated. The 2PDOS for processes corresponding to the sum and the difference of two phonons with opposite wave vectors are the essential tools to analyze the influence of pressure on the phonon linewidths, attributed to pressure-induced changes in the anharmonic decay rate of two-phonon processes [14]. Additional details of these calculations for this particular compound were reported in Ref. [4].

III. RESULTS AND DISCUSSION

A. Raman modes under hydrostatic pressure

Figure 1 displays representative Raman spectra at different pressures between 0 and 6 GPa for both a-plane and c-plane samples in the spectral region between 400 and 750 cm^{-1}. In the a-plane sample all active Raman modes are simultaneously observed despite the fact that in this scattering geometry the only allowed optical modes are the E_2^{high}, E_2^{low}, $A_1(TO)$, and $E_1(TO)$. However, the $A_1(LO)$ and $E_1(LO)$ are also observed due to deviations from normal incidence conditions in the incident laser beam path caused by the large angular aperture of the focusing objective (NA = 0.35), leading to relaxation of Raman selection rules. Incidentally, we rule out any mode mixing effect due to the small effective light cone for collection, which is ≈8° due to the large refractive index of diamond in this spectral range. In addition, the residual

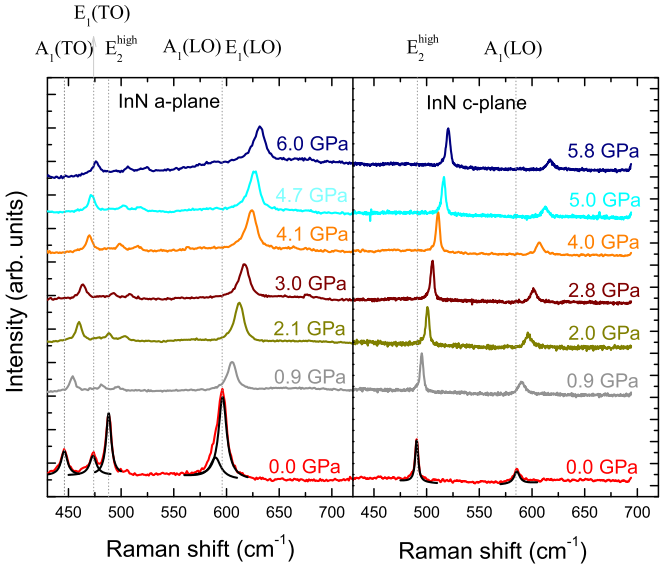

FIG. 1. Raman spectra of an a-plane and c-plane InN epilayer at different pressures and at room temperature. The spectra were vertically shifted for clarity. The full lines show representative least-squares fits to the Raman spectra using Lorentzian line shapes at ambient pressure.

n-type doping also contributes to the partial suppression of the Raman selection rules through impurity scattering. Although this allows for the observation of all Raman modes in the same experimental configuration, the spectral position of the LO modes cannot be unequivocally determined solely from the spectra of the a-plane sample. This hampers the precise determination of the LO-TO splitting and, thus, of e_T^* which is the key quantity we aim to investigate. On the other hand, in the c-plane sample only the E_2^{high} and $A_1(LO)$ are observed. This enables us to overcome the difficulties in the determination of the spectral position of the LO modes. Instead of going through a data deconvolution process, we precisely obtain the frequency of the $A_1(LO)$ as a function of pressure from the Raman spectra of the c-plane sample. These values are then used as input parameters to determine the pressure dependence of the $E_1(LO)$ in the a-plane sample. The perfect match of the E_2^{high} mode frequencies measured in both samples was used to validate such a procedure.

Figure 2(a) displays the spectral position of the A_1, E_1, and E_2^{high} modes as a function of pressure as determined from the Raman spectra of Fig. 1. The dashed lines represent fits to the data points using linear functions. The full symbols

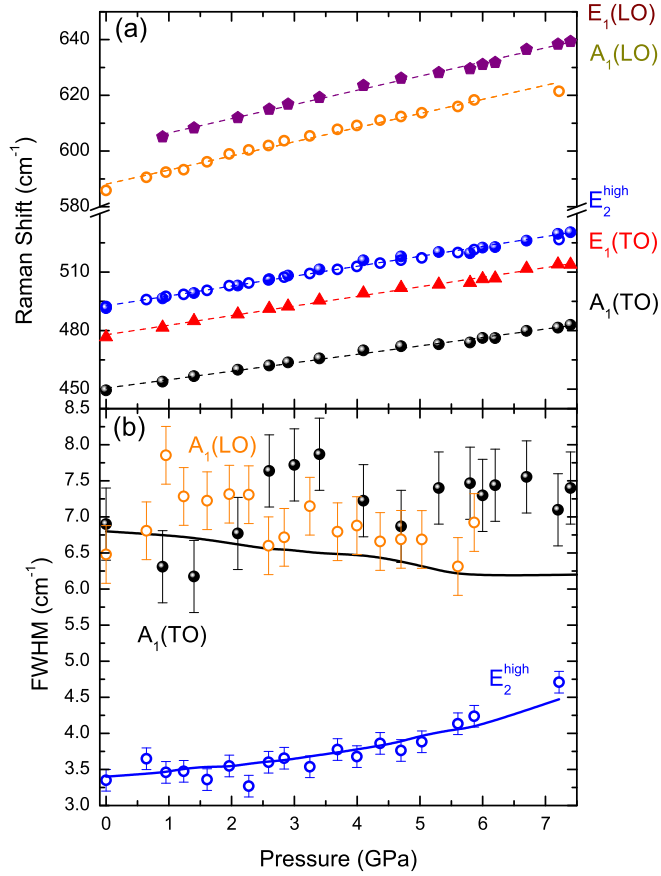

FIG. 2. (a) Pressure dependence of the zone-center optical phonons of wurtzite InN measured by Raman scattering. Solid lines are results of least-squares fits to the data points using linear relations. The full (open) symbols correspond to the a-plane (c-plane) sample. (b) Full width at half maximum (FWHM) for the E_2^{high}, $A_1(TO)$, and $A_1(LO)$ modes. The solid lines represent results of the calculations based on the Fermi-resonance model.

TABLE I. Coefficients from the fits to the data in Fig. 2 using the expression $\omega_s = \omega_0\ (\mathrm{cm}^{-1}) + (\partial\omega/\partial P)\ (\mathrm{cm}^{-1}/\mathrm{GPa})P$. The values within brackets correspond to *ab initio* calculations within the generalized gradient approximation (GGA).

Mode	ω_0	$\partial\omega/\partial P$
E_2^{low}		(-0.67)
E_2^{high}	492.7 ± 0.2	$5.07 \pm 0.1\ (5.73)$
$A_1(\mathrm{TO})$	450.5 ± 0.2	$4.32 \pm 0.1\ (5.18)$
$E_1(\mathrm{TO})$	477.8 ± 0.2	$4.92 \pm 0.1\ (5.39)$
$A_1(\mathrm{LO})$	588.1 ± 0.2	$5.07 \pm 0.1\ (5.53)$
$E_1(\mathrm{LO})$	601.4 ± 0.2	$5.09 \pm 0.1\ (5.64)$

correspond to the measurements on the a-plane sample, whereas the open symbols correspond to the c-plane geometry. The frequency of the E_2^{high} mode as well as its pressure coefficient, $\partial\omega/\partial P$, is found to be in excellent agreement between both samples. The frequency of the $A_1(\mathrm{TO})$, $E_1(\mathrm{TO})$, and $E_1(\mathrm{LO})$ modes was extracted from the a-plane sample, whereas the $A_1(\mathrm{LO})$ mode was obtained from the c-plane sample, as mentioned before. In Table I we summarize the results obtained from the linear fits to the data points in Fig. 2(a), as well as the calculated values corresponding to the pressure coefficient of the different phonon modes (in parentheses). The experimental pressure coefficients of this work agree well with the ones previously determined [11,12], although for the TO modes the latter values tend to be slightly larger (approximately 12%) than the ones reported here.

Figure 2(b) displays the full width at half maximum (FWHM) of the E_2^{high} and A_1 modes as a function of pressure. The E_1 mode (not shown) exhibits a similar behavior as the A_1, i.e., the FWHM remains constant within the experimental uncertainty upon pressure increase. In addition, we also display with solid lines (blue and black) the FWHM obtained from the computation of the anharmonic broadening proportional to the 2PDOS, resulting from the *ab initio* calculations of the E_2^{high} and $A_1(\mathrm{TO})$ vibrational modes. In this way, we are assuming that the origin of the broadening as well as its pressure dependence is fully due to anharmonic decay. Inhomogeneous broadening can be easily ruled out since the line shapes of all modes are Lorentzian functions. The exception is the E_2^{high} mode which is better described by a Fano profile. In fact, this is the evidence that the E_2^{high} mode is strongly affected by anharmonic interactions with the two-phonon continuum. The two-phonon DOS used for the calculations of the mode linewidths, displayed in Fig. 2(b) as solid lines, are shown in Fig. 3. The functions $\rho^{\pm}$ correspond to decay processes with phonon wave vectors $k \rightarrow k' \pm k''$, thus, probing different regions of the Brillouin zone. In dashed lines we have overlapped the calculated frequency of each mode at the given pressure with $\rho^{\pm}$, which is a measure of the decay probability of each optical mode into lower energy modes. The key point is to identify regions in the 2PDOS with a different pressure coefficient as compared to that of the optical phonons. For example, the larger FWHM of the E_2^{high} as pressure increases can be explained through the enhancement of the anharmonic decay probability. This results from the fact that the edge of the 2PDOS around 450 cm^{-1} shifts

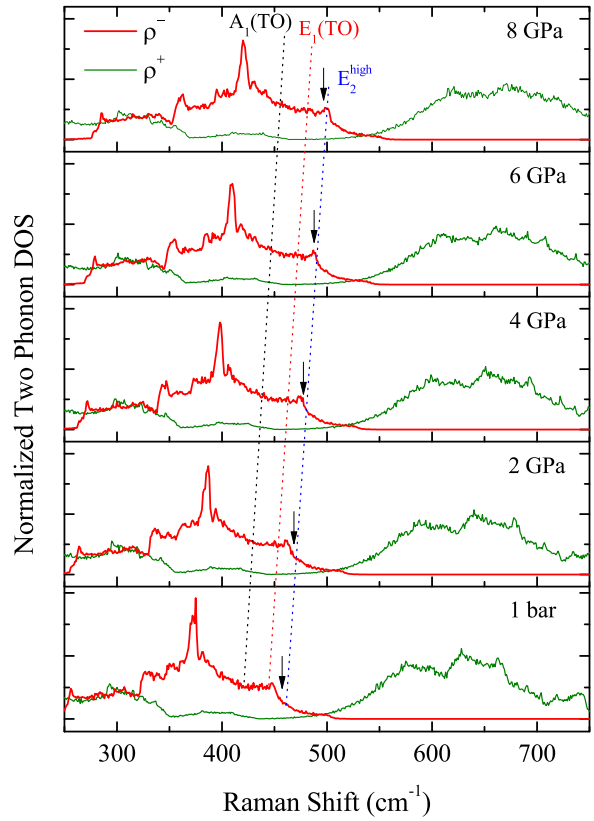

FIG. 3. *Ab inito* calculations of the two-phonon density of states (2PDOS) for selected pressures. The corresponding frequency of the $E_1(\mathrm{TO})$, $A_1(\mathrm{TO})$, and E_2^{high} is also shown with dashed lines. The arrows indicate the intersection of the E_2^{high} with the 2PDOS where strong coupling of the E_2^{high} with second-order modes can be identified. The functions $\rho^{\pm}$ correspond to decay processes with phonon wave vectors $k \rightarrow k' \pm k''$.

to higher energies with a larger pressure coefficient than the E_2^{high}. As a consequence, the FWHM of the E_2^{high} increases with pressure as shown in Fig. 2(b). Also in good agreement with the experiment, for the $A_1(\mathrm{TO})$ and $E_1(\mathrm{TO})$ modes the calculations do show that the linewidth is essentially pressure independent. The reason is that the 2PDOS does not exhibit any substantial increase in the frequency region of these modes at all studied pressures.

B. Transverse effective charge

Figure 4(a) displays the pressure dependence of the LO-TO splitting for the A_1 and E_1 modes (strictly speaking we plot the difference of the squared frequencies, as needed in Eq. (1) to evaluate e_T^*). In both cases the splitting increases with pressure but at a much stronger pace than for AlN and GaN [8]. The transverse effective charge as computed with Eq. (1) for InN (symbols and solid lines) is shown in Fig. 4(b) in its normalized form as $e_T^*(P)/e_T^*(0)$. The normalization is necessary for the comparison with other materials (dashed lines), namely, GaN [8], AlN [8], GaAs[26], ZnO [9], and SiC [7]. In spite of the strong increase of the LO-TO splitting, for InN both A_1 and E_1 modes the transverse effective charge decreases under pressure. As discussed below, the

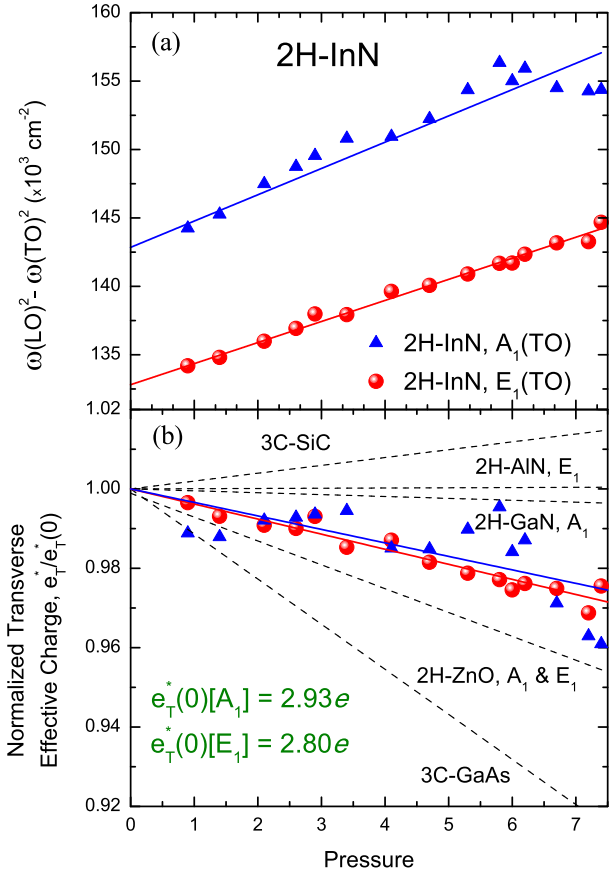

FIG. 4. (a) Hydrostatic pressure dependence of the LO-TO splittings for the polar A_1 and E_1 modes. Solid lines are results of least-squares fits to the data points using linear relations. (b) Normalized transverse effective charge for both InN polar modes as well as the corresponding data for GaN, AlN, GaAs, ZnO, and SiC.

magnitude and sign of its pressure coefficient fits very well into the previously observed systematics as a function of bond ionicity. Before this we shall examine the different contributions to the reduction of e_T^* with pressure in wurtzite InN, which for the E_1 mode corresponds to a coefficient of $-0.9 \times 10^{-2} e_0$/GPa (in units of the electron elementary charge). The large positive contribution from the LO-TO splitting ($+3.4 \times 10^{-2} e_0$/GPa) is effectively overcompensated by the reduction of the unit-cell volume ($-1.7 \times 10^{-2} e_0$/GPa), as obtained from Murnaghan's equation of state [27] and the elastic constants reported in Ref. [28], but mainly by the large negative contribution from the high-frequency dielectric constant ϵ_∞ ($-2.6 \times 10^{-2} e_0$/GPa). The latter contribution was computed using the recent determination by Oliva *et al.* [5] based on optical interferences measurements, yielding $\partial \epsilon_\infty / \partial P = -8.8 \times 10^{-2}$ GPa^{-1}. Totally similar numbers are obtained for the A_1 mode.

At this stage, we would like to rule out an effect that, in principle, can spoil the accurate determination of the pressure dependence of the transverse effective charges, namely the fact that in InN the frequency of the A_1(LO) and E_1(LO) Raman modes varies as the laser excitation energy changes. Such a behavior was ascribed to the occurrence of double-resonance processes, that dominate the Raman scattering by LO phonons with large wave vectors, due to the peculiar electronic band structure of InN [13]. Without going further into details, a similar effect regarding the changes in the resonance conditions might be expected if the laser excitation energy remains constant but the whole band structure changes through the application of pressure, as in our case. In the pressure range of our experiments (approximately 8 GPa), the band gap of InN varies by about 260 meV [29]. The same detuning from the resonance condition is attained at ambient pressure by exciting with a laser energy of 2.15 eV, instead of the 2.41 eV of the green Ar line. Using the experimental results of Ref. [13], the frequency shift of both LO modes from the resonance effect amounts at most to 2 cm^{-1}, whereas the total hydrostatic pressure-induced shift is 41 cm^{-1}. As a consequence and in the worst-case scenario, we would overestimate the pressure coefficient of the transverse effective charge by less than 2%.

As illustrated in Fig. 4(b), there is a clear trend in the pressure derivative of e_T^* for the several tetrahedrally bonded polar semiconductor compounds. To unravel the nature of such systematics, one would have to dig into the underlying physics of the transverse effective charge and its dependence on interatomic distance. The transverse effective charge is the magnitude that determines the strength of the absorption of electromagnetic radiation by transverse optical phonons in polar solids. Far infrared light propagates in a polar medium in the form of optical-phonon polaritons. The frequency of the upper phonon-polariton branch in the long-wavelength limit corresponds to that of the longitudinal-optical phonon ($\omega_{\rm LO}$), which splits up from $\omega_{\rm TO}$ due to a macroscopic polarization induced by the self-sustained longitudinal vibrations of the polar lattice. This splitting can be associated with the transverse effective charge, as described by Eq. (1), using the Lyddane-Sachs-Teller relation to express the static and high-frequency dielectric constants in terms of the optical-phonon frequencies [30]. Despite being a dynamical concept, e_T^* is intimately related to the bond polarity [31]. The latter is a ground-state property of the polar lattice linked to the (static) increment in electronic density around the anion, due to its larger electron affinity as compared to the cation. For the purpose of the present discussion, instead of bond polarity, we prefer to use the closely related bond ionicity f_i, which is clearly defined within the dielectric theory of the covalent bond by Phillips and Van Vechten [32]. Figure 5 displays the magnitude and sign of the linear pressure coefficient of e_T^* as a function of bond ionicity for the five compounds considered before, together with available data for their counterparts of different common-cation families.

We consider first the series of compounds SiC, AlN, GaN, InN, and ZnO, in order of higher bond ionicity, for which the anion is an atom from the first row of the periodic table. With increasing pressure there is an increased overlap between the valence electrons of the cation and the core electrons of the anion as compared to the situation at ambient conditions. The small difference in electronegativity between Si and C leads in SiC to a small ionicity as well as effective charge. With decreasing interatomic distance, additional charge flows from Si to C, thus increasing e_T^* and giving a positive pressure

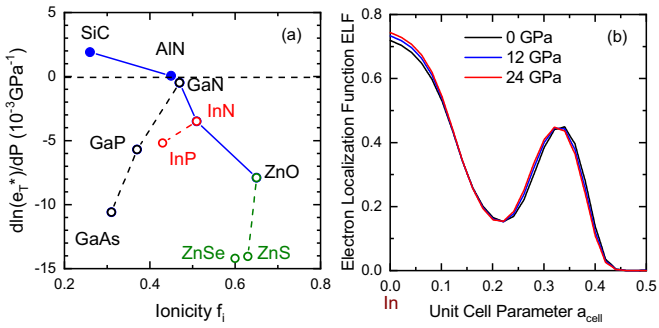

FIG. 5. (a) The pressure derivative of the logarithm of the transverse effective charge as a function of the bond ionicity for several group-IV, III–V, and II–VI semiconductor compounds. The parameters needed for the calculation of the pressure coefficient of the transverse effective charges were obtained from this work and the literature [6,8,9,33,34]. (b) Values of the electron localization function (ELF) calculated in real space using *ab initio* pseudopotentials for three different pressures. The In atom is at the origin of the unit cell.

coefficient. However, the pressure derivative of e_T^* changes sign and its reduction becomes stronger with larger bond ionicity. This effect is just due to Pauli's exclusion principle. As the interatomic distance diminishes under pressure, the valence electrons of the cation would be increasingly repelled by the core electrons of the anion. Hence, part of the previously transferred charge will "flow back" from the anion to the cation, leading to a net reduction of e_T^* under pressure. Of course, the effects of Pauli's repulsion are the weakest for the compounds with anions from the first row of the periodic table (symbols connected by solid lines in Fig. 5), because there are no p electrons in the core of the anions. These compounds (SiC, AlN, GaN, InN, ZnO) thus exhibit a smaller pressure coefficient of e_T^* as compared with other members of the corresponding common-cation family (symbols connected by dashed lines in Fig. 5). With increasing row number (going from N to P to As for III-V and from O to S to Se for II–VI compounds) the radius of the anion cores increases and so does the Pauli repulsion against the valence electrons transferred from the cation. As a consequence, in spite of the decrease in bond ionicity, the pressure-induced reduction of e_T^* becomes more pronounced for increasing anion core radius, as observed in Fig. 5. Further investigation of BN will provide a complete picture for this phenomenon, since for BN e_T^* is expected to increase under pressure such as for SiC, due to its less ionic bond character.

Finally, to support the interpretation given above for the behavior of the transverse effective charges under pressure, we have extracted from the *ab initio* calculations the so-called electron localization function (ELF). Within the pseudopotential formalism, the ELF represents the probability density corresponding solely to the valence electrons (core electrons are not included). In Fig. 5(b), the ELF of InN is plotted in the unit-cell half centered at the In atom, the cation, for three different pressures. As pressure increases, it is clear that the valence charge density increases around the cation, indicating a reduction of the bond ionicity, as assumed before to explain the reduction of the transverse effective charge.

IV. CONCLUSIONS

In summary, we have studied the hydrostatic pressure dependence of the first-order Raman modes in wurtzite InN up to 8 GPa. We have addressed the pressure coefficient of the optical modes and, in particular, their linewidth. The *ab initio* lattice-dynamical calculations were instrumental for unraveling the origin of the anomalous broadening of the nonpolar E_2^{high} mode, which was found to be due to a pressure-induced enhancement of the two-phonon decay rate. Such an enhancement arises from an incremental tuning-into-resonance of the E_2^{high} frequency with a steep edge in the two-phonon density of states at around 460 cm^{-1}, as pressure increases. For the other optical modes no major effect in the linewidth was experimentally observed, in good agreement with theory which does not predict any resonant behavior as for the E_2^{high} mode. We have also performed a comparative study of the influence of pressure on the transverse effective charge for the A_1 and E_1 modes. The outcome of this study is that the magnitude and sign of $|\partial e_T^*/\partial P|$ depends at last on the strength of the Pauli repulsion between the valence charge density transferred from the cations to the anions and the anion core-electron density. For compounds with anions belonging to the first row of the periodic table this implies that, as the bond ionicity increases, the pressure-induced change in transverse effective charge is more pronounced, changing sign from positive to negative for $f_i \approx 0.46$. For compounds with a common cation the pressure-induced reduction of e_T^* is determined by anion core radius. These conclusions are further supported by the *ab initio* calculations of the electron localization function performed here as a function of pressure.

ACKNOWLEDGMENTS

The Spanish Ministerio de Economía, Industria y Competitividad is gratefully acknowledged for its support through Grant No. SEV-2015-0496 in the framework of the Spanish Severo Ochoa Centre of Excellence program and through Grants No. MAT2015-70850-P (HIBRI2), No. CSD2010-00044 (Consolider NANOTHERM), and No. MAT2017-90024-P (TANGENTS)-EI/FEDER, UE. This work used the Extreme Science and Engineering Discovery Environment (XSEDE), which is supported by National Science Foundation Grant No. OCI-1053575. Additionally, the authors acknowledge the support from Texas Advances Computer Center (TACC) and the Bridges supercomputer at Pittsburgh Supercomputer Center. A.H.R. acknowledges the support from National Science Foundation (NSF) DMREF-NSF 1434897 and DOE DE-SC0016176 projects. The Deutsche Forschungsgemeinschaft (DFG, German research foundation) within the Collaborative Research Center Semiconductor Nanophotonics (CRC 787) is gratefully acknowledged. S.J.C. and J.S.S. acknowledge support from AFOSR and ONR.

[1] S. Krukowski, A. Witek, J. Adamczyk, J. Jun, M. Bockowski, I. Grzegory, B. Lucznik, G. Nowak, M. Wróblewski, A. Presz, S. Gierlotka, S. Stelmach, B. Palosz, S. Porowski, and P. Zinn, J. Phys. Chem. Solids **59**, 289 (1998).

[2] C. Pinquier, F. Demangeot, J. Frandon, J. W. Pomeroy, M. Kuball, H. Hubel, N. W. A. van Uden, D. J. Dunstan, O. Briot, B. Maleyre, S. Ruffenach, and B. Gil, Phys. Rev. B **70**, 113202 (2004).

[3] Z. G. Qian, W. Z. Shen, H. Ogawa, and Q. X. Guo, J. Phys.: Condens. Matter **16**, R381 (2004).

[4] J. Serrano, A. Bosak, M. Krisch, F. J. Manjón, A. H. Romero, N. Garro, X. Wang, A. Yoshikawa, and M. Kuball, Phys. Rev. Lett. **106**, 205501 (2011).

[5] R. Oliva, A. Segura, J. Ibáñez, T. Yamaguchi, Y. Nanishi, and L. Artús, Appl. Phys. Lett. **105**, 232111 (2014).

[6] A. R. Goñi, F. Kaess, J. S. Reparaz, M. I. Alonso, M. Garriga, G. Callsen, M. R. Wagner, A. Hoffmann, and Z. Sitar, Phys. Rev. B **90**, 045208 (2014).

[7] D. Olego, M. Cardona, and P. Vogl, Phys. Rev. B **25**, 3878 (1982).

[8] A. R. Goñi, H. Siegle, K. Syassen, C. Thomsen, and J.-M. Wagner, Phys. Rev. B **64**, 035205 (2001).

[9] J. S. Reparaz, L. R. Muniz, M. R. Wagner, A. R. Goñi, M. I. Alonso, A. Hoffmann, and B. K. Meyer, Appl. Phys. Lett. **96**, 231906 (2010).

[10] C. Pinquier, F. Demangeot, J. Frandon, J. C. Chervin, A. Polian, B. Couzinet, P. Munsch, O. Briot, S. Ruffenach, B. Gil, and B. Maleyre, Phys. Rev. B **73**, 115211 (2006).

[11] J. Ibáñez, F. J. Manjón, A. Segura, R. Oliva, R. Cuscó, R. Vilaplana, T. Yamaguchi, Y. Nanishi, and L. Artús, Appl. Phys. Lett. **99**, 011908 (2011).

[12] J. Ibáñez, R. Oliva, F. J. Manjón, A. Segura, T. Yamaguchi, Y. Nanishi, R. Cuscó, and L. Artús, Phys. Rev. B **88**, 115202 (2013).

[13] V. Yu. Davydov, A. A. Klochikhin, A. N. Smirnov, I. Yu. Strashkova, A. S. Krylov, H. Lu, W. J. Schaff, H.-M. Lee, Y.-L. Hong, and S. Gwo, Phys. Rev. B **80**, 081204(R) (2009).

[14] C. Ulrich, E. Anastassakis, K. Syassen, A. Debernardi, and M. Cardona, Phys. Rev. Lett. **78**, 1283 (1997).

[15] F. J. Manjón, J. Serrano, I. Loa, K. Syassen, C. T. Lin, and M. Cardona, Phys. Rev. B **64**, 064301 (2001).

[16] J. Serrano, A. H. Romero, F. J. Manjón, R. Lauck, M. Cardona, and A. Rubio, Phys. Rev. B **69**, 094306 (2004).

[17] H. K. Mao, J. Xu, and P. M. Bell, J. Geophys. Res. **91**, 4673 (1986).

[18] W. Kohn and L. J. Sham, Phys. Rev. **140**, A1133 (1965).

[19] P. Hohenberg and W. Kohn, Phys. Rev. **136**, B864 (1964).

[20] Gonze, Phys. Rev. A **52**, 1096 (1995).

[21] X. Gonze, G. Rignanese, M. Verstraete, J. Beuken, Y. Pouillon, R. Caracas, F. Jollet, M. Torrent, G. Zerah, M. Mikami, P. Ghosez, M. Veithen, J. Raty, V. Olevano, F. Bruneval, L. Reining, R. Godby, G. Onida, D. Hamann, and D. Allan, Z. Kristallogr. **220**, 558 (2005).

[22] X. Gonze, B. Amadon, P.-M. Anglade, J.-M. Beuken, F. Bottin, P. Boulanger, F. Bruneval, D. Caliste, R. Caracas, M. Côté, T. Deutsch, L. Genovese, P. Ghosez, M. Giantomassi, S. Goedecker, D. Hamann, P. Hermet, F. Jollet, G. Jomard, S. Leroux *et al.*, Comput. Phys. Commun. **180**, 2582 (2009).

[23] X. Gonze, F. Jollet, F. Abreu Araujo, D. Adams, B. Amadon, T. Applencourt, C. Audouze, J.-M. Beuken, J. Bieder, A. Bokhanchuk, E. Bousquet, F. Bruneval, D. Caliste, M. Côté, F. Dahm, F. Da Pieve, M. Delaveau, M. Di Gennaro, B. Dorado, C. Espejo *et al.*, Comput. Phys. Commun. **205**, 106 (2016).

[24] J. P. Perdew, K. Burke, and M. Ernzerhof, Phys. Rev. Lett. **77**, 3865 (1996).

[25] M. Fuchs and M. Scheffler, Comput. Phys. Commun. **119**, 67 (1999).

[26] M. Cardona, J. Phys. Colloq. **45**, C8-29 (1984).

[27] F. D. Murnaghan, Proc. Natl. Acad. Sci. USA **30**, 244 (1944).

[28] R. J. Jiménez-Riobóo, R. Cuscó, N. Domènech-Amador, C. Prieto, T. Yamaguchi, Y. Nanishi, and L. Artús, Phys. Status Solidi RRL **6**, 256 (2012).

[29] P. Perlin, V. Iota, B. A. Weinstein, P. Wisniewski, T. Suski, P. G. Eliseev, and M. Osinski, Appl. Phys. Lett. **70**, 2993-2995 (1997).

[30] P. Y. Yu and M. Cardona, *Fundamentals of Semiconductors* (Springer, Berlin, 1996), pp. 285–295.

[31] W. A. Harrison, *Electronic Structure and the Properties of Solids* (Dover, New York, 1989), pp. 218–224.

[32] J. A. Van Vechten, Phys. Rev. **182**, 891 (1969).

[33] B. A. Weinstein and R. Zallen, *Light Scattering in Solids IV*, edited by M. Cardona and G. Güntherodt (Springer, Berlin, 1984), pp. 463–525, and references therein.

[34] S. Adachi, *Properties of Group-IV, III-V and II-VI Semiconductors* (Wiley, West Sussex, 2005), pp. 73–93, and references therein.